# Towards automatic resistance evaluation using mesh adaptation

Jeroen Wackers, Ganbo Deng, Alban Leroyer, Clémence Raymond, Jules Richeux

▶ **To cite this version:**

Jeroen Wackers, Ganbo Deng, Alban Leroyer, Clémence Raymond, Jules Richeux. Towards automatic resistance evaluation using mesh adaptation. 24th Numerical Towing Tank Symposium (NuTTS 2022), Oct 2022, Zagreb, Croatia. hal-03709367

**HAL Id: hal-03709367**
**https://hal.science/hal-03709367**

Submitted on 29 Jun 2022

**HAL** is a multi-disciplinary open access archive for the deposit and dissemination of scientific research documents, whether they are published or not. The documents may come from teaching and research institutions in France or abroad, or from public or private research centers.

L'archive ouverte pluridisciplinaire **HAL**, est destinée au dépôt et à la diffusion de documents scientifiques de niveau recherche, publiés ou non, émanant des établissements d'enseignement et de recherche français ou étrangers, des laboratoires publics ou privés.

# Towards automatic resistance evaluation using mesh adaptation

**Jeroen Wackers, Ganbo Deng, Alban Leroyer, Clémence Raymond, and Jules Richeux**
LHEEA, Ecole Centrale de Nantes/CNRS UMR 6298, Nantes/France
jeroen.wackers@ec-nantes.fr

## 1 Introduction

Today, mesh generation is a bottleneck for the continuing growth of CFD for realistic simulation in research and industry (Slotnick et al. (2014)). Meshing requires more expert user knowledge than any other aspect of numerical simulation, while the trend towards more complex simulations implies that even experts cannot determine beforehand what mesh fineness, in what positions, is needed to resolve the main flow features correctly. Thus, computations may need to be repeated several times, leading to unpredictable costs and turnaround times, which is an obstacle for large-scale use in industry.

Adaptive mesh refinement, which locally refines the mesh during the simulation according to the requirements of the flow, is a natural solution to these problems. However, mesh adaptation is only acceptable in an industrial context if makes computations not only more accurate, but also simpler; it should be performed automatically, with little or no user intervention, and be robust enough to produce reliable solutions for a large range of test cases.

Apart from a powerful and reliable adaptive meshing technique, this requires standardised guidelines to set the simulation parameters correctly for each simulation, independent of the flow conditions and the geometry. Wackers et al. (2022) show that for calm-water resistance of model-scale bare hulls, such user guidelines exist. Starting from this result, the current paper investigates if such protocols can be developed for calm-water resistance in other situations. If this is true, adaptive refinement for resistance evaluation is mature enough to envisage industrial application.

After presenting our flow solver ISIS-CFD and its mesh adaptation (section 2), the paper summarises the guidelines of Wackers et al. (2022) in section 3. Then section 4 applies the protocol to resistance simulations with different geometries and physics. Implications of these tests are discussed in section 5.

## 2 ISIS-CFD and adaptive refinement

The Navier-Stokes solver ISIS-CFD developed at ECN – CNRS, available in the FINE™/Marine computing suite from Cadence Design Systems, is an incompressible unstructured finite-volume solver for multifluid flow. The velocity field is obtained from the momentum conservation equations and the pressure field is extracted from the mass conservation constraint transformed into a pressure equation. Free-surface flow is simulated with a conservation equation for the volume fraction of water, discretized with specific compressive discretization schemes. The unstructured discretization is face-based. Therefore, cells with an arbitrary number of arbitrarily-shaped constitutive faces are accepted, which enables for example adaptive mesh refinement. The code is fully parallel using the message passing interface (MPI) protocol. A list of references concerning the solver can be found in Wackers et al. (2022).

Mesh adaptation in ISIS-CFD (Wackers et al. (2017)) is performed by local division of unstructured hexahedral meshes, created with the mesher Hexpress. The adaptation is included in the flow solver and fully parallelised. The decision where to refine comes from a metric refinement criterion (see e.g. Alauzet and Frazza (2021)), a tensor field $C(x, y, z)$ based on the water surface position and on second derivatives of the flow variables, which give a crude indication of the local truncation errors. The grid is refined until the dimensions $\mathbf{d}_{i,j}$ ($j = 1, 2, 3$) of each hexahedral cell $i$ satisfy:

$$\|C_i \, \mathbf{d}_{i,j}\| = T_r. \tag{1}$$

The refinement criterion based on the second derivatives of the flow is not very sensitive to grid refinement, so the cell sizes everywhere are proportional to the constant threshold $T_r$.

The refinement criterion must react to all the flow features which are relevant for ship resistance. This implies a combination of a free-surface capturing criterion and the Hessian of the pressure, which is a suitable indicator of the orbital flow fields in the waves. Also the accurate resolution of the boundary

layer and wake is needed to correctly predict both viscous and pressure forces, which suggests refinement based on the velocity Hessians. The combined free-surface and flux-component Hessian criterion of Wackers et al. (2017) is therefore adopted. Figure 1 shows a mesh generated with this criterion: combined refinement at and below the surface can be seen in waves, while the mesh around the hull is refined at the bow and in the boundary layer. Figure 2 compares the original and adapted meshes.

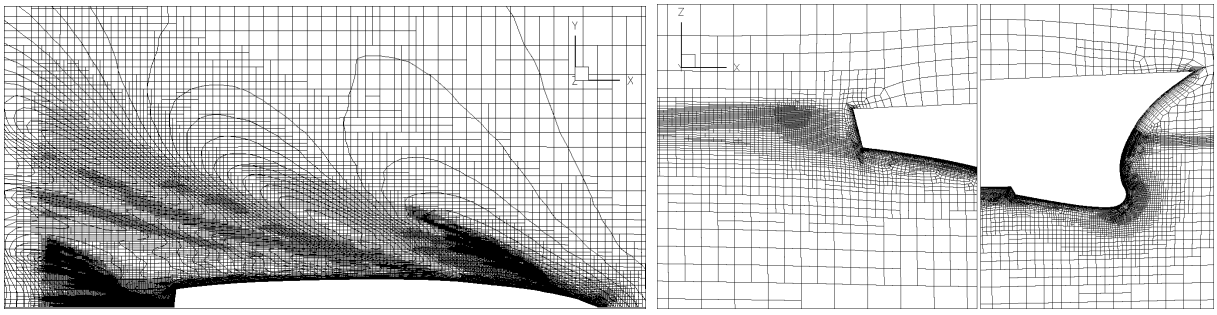

Fig. 1: Example adapted mesh following the current protocol: free surface and details of the $Y$-symmetry plane. The case is the DTMB 5415 at $Fr = 0.41$ of section 4.1, with $T_{rH} = 0.07$.

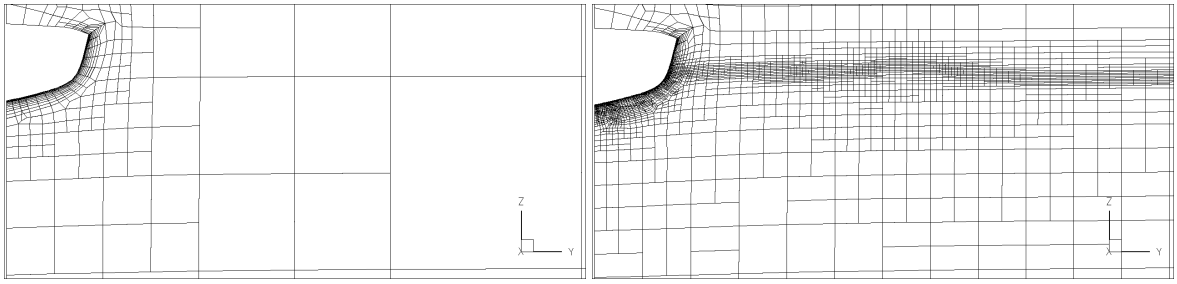

Fig. 2: Original and adapted mesh in an X-cut near the stern for the DTMB 5415.

## 3 Protocol for mesh refinement settings

For routine simulation, default values for the simulation parameters are needed, which must be straightforward and correct, without a need for trial and error. These guidelines have to be valid over a range of ship lengths, velocities, hull shapes, etc. Our approach to defining guidelines is to use physical arguments, notably dimensional analysis, to reduce the number of input variables that have to be considered and then to apply experience and systematic testing to find sensible guidelines for the remaining parameters.

The threshold $T_r$ of equation (1) is important since it determines the mesh density. At the free surface, we wish to specify target cell sizes in terms of the ship length $L$. Therefore, the free-surface refinement criterion is defined with unit vectors in equation (1), so its threshold $T_{rS}$ equals the desired cell size normal to the free surface, which is chosen as $L/1000$ following established ISIS-CFD guidelines.

To keep the criteria compatible, a similar behaviour is sought for the Hessian refinement criterion: the mesh density on the hull should be proportional to the threshold value, independent of the case parameters. Therefore, the criterion is non-dimensionalized using the reference length and velocity. As a result, the choice for $T_{rH}$ no longer depends on the ship length and velocity; only a (weak) dependence on $Fr$, $Re$, and the hull shape remains, which can be ignored for a specific class of ship hulls (such as displacement hulls). Our tests suggest the range $T_{rH} \in [0.2L,\ 0.025L]$ for coarse to fine grids.

Other parameters are also expressed in terms of $L$. For example, the resolution of small flow details can be controlled by specifying a minimum cell size, below which cells are no longer refined. For resistance simulations, which do not need these details, a large minimum cell size of $L/1000$ is preferable. Furthermore, resolving the ship wake and the wave field far behind the ship is not needed for resistance computations, so horizontal refinement is forbidden aft of $0.3L$ behind the stern: this removes the far wake field, but does not significantly alter the forces while reducing the number of cells by up to 40%.

## 4 How general is the protocol?

To test the protocol, it is applied successively to cases which are further and further away from those for which it was developed. Results are compared with experiments and simulations on non-adapted meshes.

### 4.1 Model-scale bare hulls

The first test concerns three towed models which span the scale of bare displacement hulls: the DTMB 5415 at $Fr = 0.41$ and $Re = 1.74 \cdot 10^7$ (Olivieri et al. (2001)), the KCS at $Re = 1.257 \cdot 10^7$ and $Fr = 0.260$ and KVLCC2 at $Fr = 0.14232$ and $Re = 4.6 \cdot 10^6$ (Kim et al. (2001)). Wall laws are used and the turbulence model is $k - \omega$ SST, except for the KVLCC2 which uses EASM. The results are compared with simulations on Hexpress meshes created with the C-Wizard automatic setup tool, which provides uniform cell sizes over the hull. For a second non-adapted series, the three coarsest grids are generated by Hexpress, using manual refinement at the bow and stern. The finest grids are created from these coarser grids by refining all cells once. The full setup for all these cases is given in Wackers et al. (2022).

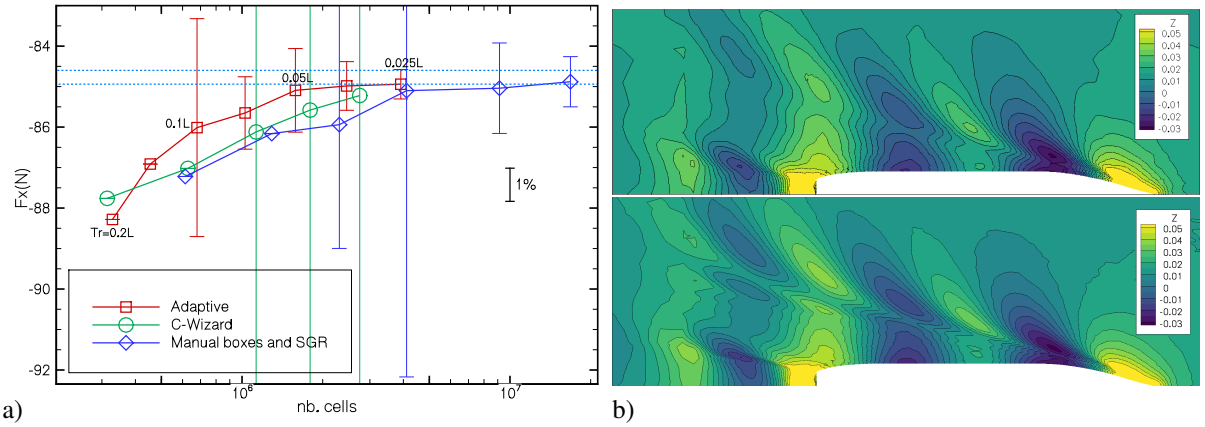


Fig. 3: KCS resistance, grid convergence and numerical uncertainty with uncertainty interval of the experimental results (a). Convergence of free-surface elevation (b), top: $T_{rH} = 0.2L$, bottom: $0.025L$.

Figures 3a and 4 shows that the resistance makes sense for all cases and that the grid convergence with the Hessian threshold $T_{rH}$ is excellent: the forces converge for lower numbers of cells than on the non-adapted meshes. The numerical uncertainty evaluated following Eça and Hoekstra (2014) confirms this: the uncertainty estimations overlap for the finer grids and are much smaller than for the non-adapted meshes. Fig. 3b shows that the local flow also converges with $T_{rH}$. Thus, varying $T_{rH}$ is an effective way to obtain grid convergence and the selected range for $T_{rH}$ is appropriate for all three cases.

The agreement with experiments is good in all cases; however, the non-adapted meshes systematically correspond better. These differences however have been traced to physical inaccuracies in the

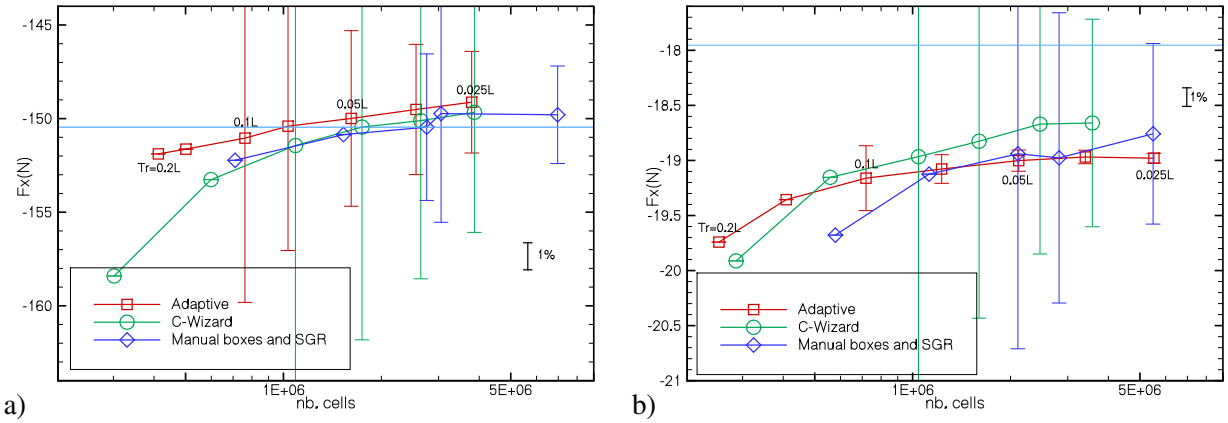


Fig. 4: Convergence of resistance for the DTMB 5415 (a) and KVLCC2 (b).

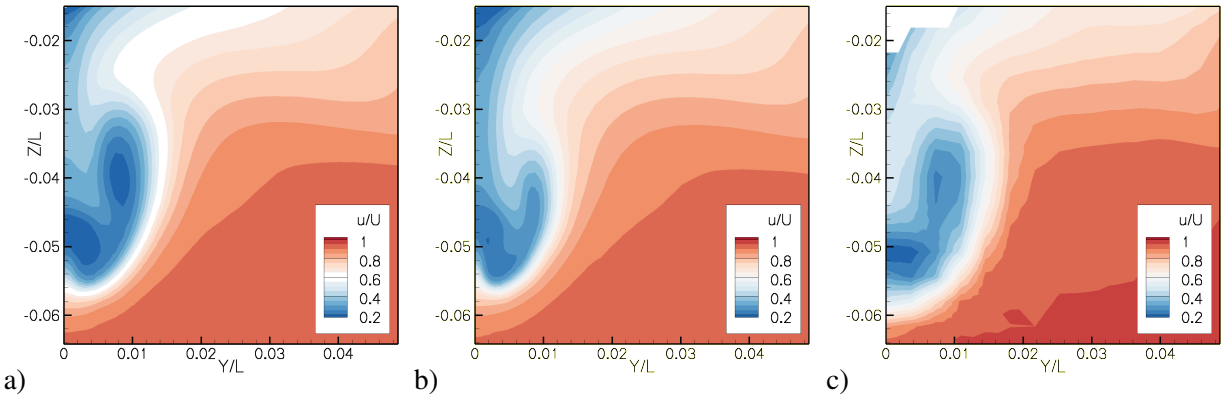


Fig. 5: KVLCC2 axial velocity in the propeller plane for wall-law solutions. Adaptive $T_{rH} = 0.025L$ (a), C-Wizard $3.6M$ cells (b) and experiments (c).

non-adapted solutions. For the DTMB 5415, only the adapted meshes capture the strong breaking bow wave, and for the KVLCC2 the non-adapted meshes fail to resolve the hook-shaped wake (Fig. 5) while the adapted grids reproduce it correctly. Altogether, the adapted-grid solutions seem more reliable.

### 4.2 Wall-resolved and full scale

To challenge the boundary treatment of the refinement protocol, the KVLCC2 case is repeated with two changes: wall-resolved model scale and wall-law full scale at $Re = 2.03 \cdot 10^9$ and $y^+ = 300$. For the wall-resolved model scale, the adaptation works like for the wall law: the convergence is good (Fig. 6a) although a few oscillations lead to larger uncertainties than for the wall law. For this more accurate boundary treatment, the adapted-grid solution is now closest to the experiments, which suggests that the result in section 4.1 is an artefact of the wall law boundary condition.

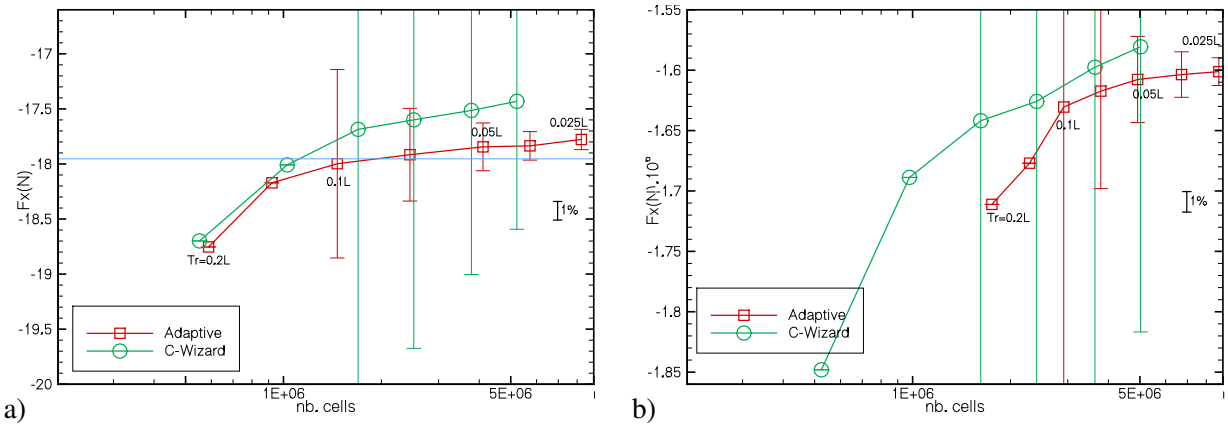


Fig. 6: KVLCC2 resistance, model-scale wall-resolved (a) and full-scale (b) simulations.

The full-scale simulations are more difficult. The flows are dominated by the pressure and harder to solve, which impacts the convergence (Fig. 6b). For the adapted series, the number of cells increases since the thinner boundary layers with higher second derivatives create more Hessian-based refinement. Therefore, the protocol would likely benefit from a modified refinement criterion for such high Reynolds numbers. Still, the convergence and uncertainty are better than for the uniform Hexpress grid series, which shows that the current protocol works for full scale.

### 4.3 Self-propulsion

Another case for which the protocol was never intended, is the KCS in self-propulsion (Hino (2005)) with a body-force model to represent the propeller. This is a challenge since the mesh refinement has never been tested for a force field before. Also, a ship propeller is tiny with respect to the ship itself. Can something so small be captured by mesh adaptation that is configured for the flow around the ship?

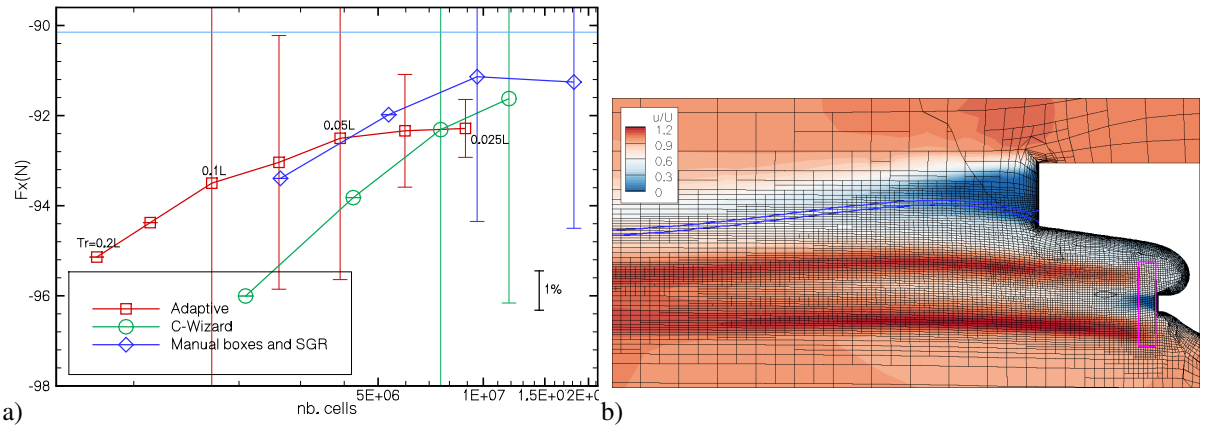


a) b)

Fig. 7: KCS self-propulsion: resistance, grid convergence for three meshing strategies and estimated numerical uncertainty (a); the blue line represents the experimental result from Hino (2005). Axial velocity in the $y$-symmetry plane (b) for $T_{rH} = 0.1L$ and location of the body force (pink box).

The initial Hexpress mesh is equal to the one from section 4.1, no particular refinement is applied around the actuator disk. Still, the adapted grid (figure 7b) captures the propeller flow well, even at the coarse threshold $T_{rH} = 0.1L$. Thus, refinement based on the ship length scale is appropriate for a detail like the actuator disk. All resistance results (figure 7a) agree well with the experiments; the difference between the series is similar to the KVLCC2 for example. These force results confirm that the mesh adaptation protocol can be used for self-propulsion.

### 4.4 Lifting hydrofoils

The final example shown is the simulation of lifting hydrofoils. It is evident here that the ship-based protocol cannot work, if only because the reference lengths are different: contrary to a ship, the main dimensions of a hydrofoil are larger than the relevant length scale for the boundary layer development, which is the chord. Therefore, the ship-based protocol is adjusted. The hydrofoil protocol uses the maximum chord $c$ as a reference lenght, with main parameters $T_{rS} = c/64$, $T_{rH} \in [c/2,\ c/16]$, and minimum cell size $c/256$. The limiting box is at $1c$ behind the trailing edge, but the forces are insensitive to this choice. The full description of the protocol and applications to several cases, including geometry / speed variations and fluid-structure interaction, is given by Richeux (2022).

Figure 8 provides an illustration for an L-shaped foil. The differences between the meshes are larger than for ships, since hydrofoils require very fine meshes at the leading edge to capture the pressure peaks. Thus, also the uncertainty is larger. However, the convergence is smooth and the uncertainty estimates suit the data perfectly. Robin et al. (2022) show that the accuracy can be increased by using the same protocol with body-aligned initial meshes; this is another demonstration of the versatility of the protocol.

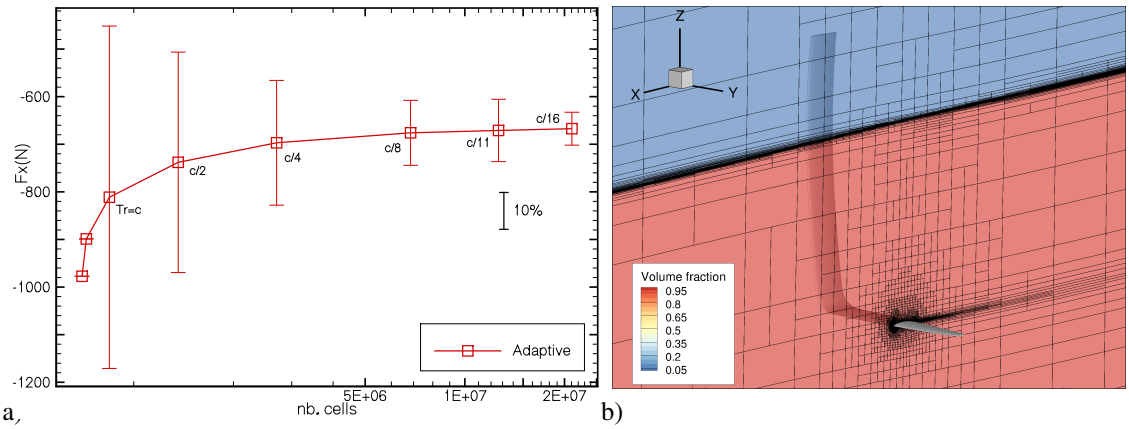


a, b)

Fig. 8: Convergence of resistance (a) and adapted mesh with water surface (b) for an L-hydrofoil.

## 5 Conclusions and discussion

How general is the mesh adaptation protocol? It provides good results for all model-scale tests, independent of the ship geometry and speed, the turbulence and wall models, and the propulsion (towed or actuator disk). It is also reasonably successful for full scale and it is likely that with minor modifications to the boundary layer treatment, the same performance as for model scale can be recovered. Finally, the hydrofoil case shows that even when the initial protocol does not apply, a similar one can be constructed that provides good reliability. Thus, routine mesh adaptation for resistance simulations is realistic today.

The grid convergence is smooth, which leads to reliable uncertainty estimations; this was also observed by Wackers et al. (2017) for mono-fluid flows and by Alauzet and Frazza (2021) for wings and aircraft using compressible flow and tetrahedral mesh adaptation. The good uncertainty estimation is likely a property of the metric-based refinement. For unstructured meshes, this is a major advantage.

Solutions on non-adapted meshes often give better resistance predictions, but the differences come from problems with these meshes, such as insufficient resolution of breaking waves and wakes. Probably, successful existing simulation methods rely to some extent on numerical / modelling error compensation to get optimal accuracy: over the years, the turbulence modelling has been tuned to work well on industrial-standard meshes. Adaptive grid refinement however reduces numerical errors by an order of magnitude with respect to fixed grids, upsetting the equilibrium of error compensation and leading to overall larger errors. Maybe the turbulence modelling must be adjusted for adaptively refined grids?

Therefore, open questions remain and the simulation protocols will probably be improved upon. Still, they have proved their generality and the potential advantages are obvious. The current results show that the principle is mature enough to start gaining experience with large-scale practical application.

## ACKNOWLEDGEMENTS

We thank the Institute Carnot MERS (ORUP project) and the research directorate of Centrale Nantes for funding the hydrofoil work, and GENCI (A0092A01308) for providing the HPC resources of CINES.

## References

F. Alauzet and L. Frazza (2021). Feature-based and goal-oriented anisotropic mesh adaptation for RANS applications in aeronautics and aerospace. *J Comp Phys*, 439:110340.

L. Eça and M. Hoekstra (2014). A procedure for the estimation of the numerical uncertainty of CFD calculations based on grid refinement studies. *J Comp Phys*, 262: 104–130.

T. Hino (Ed.) (2005). *CFD Workshop Tokyo 2005*. National Maritime Research Institute, Tokyo, Japan.

W.J. Kim, D.H. Van, and D.H. Kim (2001). Measurement of flows around modern commercial ship models. *Exp Fluids* **31**: 567–578.

A. Olivieri, F. Pistani, A. Avanzini, F. Stern, and R. Penna (2001). *Towing tank experiments of resistance, sinkage and trim, boundary layer, wake, and free surface flow around a naval combatant INSEAN 2340 model*. Technical Report 421, IIHR, Iowa.

P. Robin, A. Leroyer, D. de Premorel, J. Richeux, and J. Wackers (2022). Start with the right foot with foil'sock approach and AGR criterion. Proceedings of NuTTS 2022, Zagreb, Croatia.

J. Richeux (2022). *Towards the automation of adaptive RANS simulations for hydrofoils.* M.Sc. Thesis, Ecole Centrale de Nantes.

J. Slotnick, A. Khodadoust, J. Alonso, D. Darmofal, W. Gropp, E. Lurie, and D. Mavriplis (2014). *CFD Vision 2030 Study: A Path to Revolutionary Computational Aerosciences.* NASA/CR–2014-218178.

J. Wackers, G.B. Deng, E. Guilmineau, A. Leroyer, P. Queutey, M. Visonneau, A. Palmieri, and A. Liverani (2017). Can adaptive grid refinement produce grid-independent solutions for incompressible flows? *J Comp Phys*, 344: 364–380.

J. Wackers, G.B. Deng, C. Raymond, E. Guilmineau, A. Leroyer, P. Queutey, and M. Visonneau (2022). Adaptive grid refinement for ship resistance computations. *Ocean Eng*, 250: 110969.